

Extending Finch-Skea Isotropic Model to Anisotropic Domain in Modified $f(\mathcal{R}, \mathcal{T})$ Gravity

Tayyab Naseer ^{*} and M. Sharif [†]

Department of Mathematics and Statistics, The University of Lahore,
1-KM Defence Road Lahore-54000, Pakistan.

Abstract

This paper considers the Finch-Skea isotropic solution and extends its domain to three different anisotropic interiors by using the gravitational decoupling strategy in the context of $f(\mathcal{R}, \mathcal{T})$ gravitational theory. For this, we consider that a static spherical spacetime is initially coupled with the perfect matter distribution. We then introduce a Lagrangian corresponding to a new gravitating source by keeping in mind that this new source produces the effect of pressure anisotropy in the parent fluid source. After calculating the field equations for the total matter setup, we apply a transformation on the radial component, ultimately providing two different systems of equations. These two sets are solved independently through different constraints that lead to some new solutions. Further, we consider an exterior spacetime to calculate three constants engaged in the seed Finch-Skea solution at the spherical interface. The estimated radius and mass of a star candidate LMC X-4 are utilized to perform the graphical analysis of the developed models. It is concluded that only the first two resulting models are physically relevant in this modified theory for all the considered parametric choices.

Keywords: Anisotropy; Gravitational decoupling; Modified gravity.

PACS: 04.50.Kd; 04.40.Dg; 04.40.-b.

^{*}tayyabnaseer48@yahoo.com; tayyab.naseer@math.uol.edu.pk

[†]msharif.math@pu.edu.pk

1 Introduction

Several discoveries have recently been made by cosmologists from which it was shown that plenty of the astrophysical structures in our cosmos are not randomly arranged rather they distributed in a very organized manner. The analysis of the physical characteristics of these interstellar bodies became a topic of significant importance for researchers which helps to explain the phenomenon of accelerated cosmic expansion. It was observed from different experiments that our universe contains a big amount of a specific force that acts opposite to gravity and results in cosmic expansion. This force was named the dark energy because of its mysterious nature till now. General Relativity (\mathbb{GR}) describes this expanding phenomenon somehow, however, it faces some problems related to the cosmological constant, and thus its multiple modifications were proposed. The $f(\mathcal{R})$ theory is the first-ever generalization among them, obtained by modifying the Einstein-Hilbert action in which the Ricci scalar \mathcal{R} and its generic function are swapped by each other. Different cosmic eras like inflationary and rapid expansion phases have been discussed in this theory, and favorable outcomes were acquired [1]-[4]. The self-gravitating systems have also been discussed through several approaches in this context and found to be physically relevant [5, 6].

At that time, the geometry of spacetime and matter distribution were studied independently. Initially, Bertolami et al. [7] presented that the geometry of compact celestial objects can be well explained by taking the dependence of the above-mentioned factors on each other. In this regard, they adopted the matter Lagrangian depending on the scalar \mathcal{R} and analyzed the effects of such coupling on massive structures in $f(\mathcal{R})$ theory. Several researchers have been prompted by this idea and put their concentration to study accelerating cosmic expansion in this modified framework. Following this, physicists thought that some new insights regarding the evolution and expansion of our universe could be opened once this matter-geometry coupling is generalized at the action level. Harko et al. [8] pioneered such generalization by presenting a new theory of gravity depending on the scalar curvature and trace of the energy-momentum tensor (\mathbb{EMT}) \mathcal{T} , thus called it $f(\mathcal{R}, \mathcal{T})$ theory.

It was observed that the considered system becomes non-conserved under this modified theory in the light of which there appears an extra force (influenced by different physical factors [9]). This force alters the path of moving particles from geodesic to being in non-geodesic framework in the gravita-

tional field. Houndjo [10] used a minimal $f(\mathcal{R}, \mathcal{T})$ model to discuss cosmic eras like matter-dominated and late-time acceleration phases, and concluded that this theory supports the existing observations. Multiple minimal/non-minimal models have been proposed in this scenario, among them $\mathcal{R} + 2\xi\mathcal{T}$ gained great attention in the literature due to its linear nature. Nashed [11] discussed various pulsars in this linear gravity model and solved the differential equations by making an explicit assumption regarding the anisotropy and radial component of the metric. They found that the estimated masses of these pulsars are in accordance with the observed ones. Several other works on the stellar interiors have been done in this theory from which appealing results are obtained [12]-[16].

Within the domain of astrophysics, the exploration of compact stars stands as a captivating subject, offering valuable revelations about the fundamental properties of matter in extreme conditions. Discussing the isotropic models using standard approaches has been a primary approach in comprehending these dense systems. Nonetheless, the constraints of isotropic models become apparent when confronted with the complexities of compact celestial objects. Various cosmological surveys conducted in recent years have consistently revealed deviations from isotropy within the cosmos. Notably, investigations into inhomogeneous Supernova Ia have identified subtle discrepancies challenging the assumption of isotropy [17]-[20]. Furthermore, multiple tools, including studies of radio sources [21], and gamma-ray bursts [22], among others, have unveiled plausible inconsistencies. Migkas and Reiprich [23] recently discussed the cosmic isotropy by examining the direction-dependent X-rays emanating from massive structures. Subsequently, applying the same technique to other galaxy clusters led to the discovery that the cosmos exhibits anisotropic characteristics [24]. Hence, constructing anisotropic solutions becomes imperative in gaining insights into the cosmic origin and understanding its ultimate fate more accurately.

Finding the solution of Einstein field equations representing realistic self-gravitating system in the background of GR and modified theories becomes a crucial task for astrophysicists. These highly non-linear equations may be solved analytically, however, it is not possible to formulate such solutions in some situations, leading researchers to use numerical techniques. It is worth mentioning that the scientific community accepts only those solutions which could be used to model physically relevant interiors, i.e., all the required conditions are fulfilled. Finding an appealing strategy to solve these differential equations is itself a momentous task such that the possible resulting

outcomes would be of physical interest. In this perspective, a number of techniques have been suggested in the literature that can be used to study the nature of interior fluid distribution. Among them, a particular approach prompted physicists to use it due to its novel characteristics, referred as the gravitational decoupling. This scheme can be employed to study a compact star possessing multiple physical factors like density, pressure anisotropy, dissipation flux and shear, etc., in a very convenient way.

The innovation of this approach was established on the fact that if the field equations comprise multiple physical factors, the gravitational decoupling divides those equations in different sets corresponding to each matter source. These systems of equations are easy enough to be solved independently. Gravitational decoupling comprises two types of deformations, namely minimal and extended. The pioneering work of Ovalle [25] recently proposed the minimal geometric deformation (MGD) strategy to formulate solutions which are well agreed with the existing data of compact stars in the braneworld scenario. Subsequently, Ovalle and Linares [26] considered an isotropic self-gravitating spherical fluid interior and formulated the corresponding exact solution, showing consistency with Tolman-IV metric. Casadio et al. [27] extended this scheme to obtain the Schwarzschild spacetime in the braneworld.

An isotropic sphere has been taken into account by Ovalle and his collaborators [28] whose domain was extended to anisotropic using MGD. Sharif and Sadiq [29] extended these solutions to the Einstein-Maxwell framework to obtain two anisotropic counterparts of isotropic Krori-Barua metric and explored the effects of decoupling and charge on them. Gabbanelli et al. [30] generalized the isotropic Durgapal-Fuloria metric to anisotropic domain via MGD and concluded that the resulting models represent physically realistic compact star. A similar investigation has also been done for the isotropic Heintzmann and Tolman VII ansatz from which acceptable outcomes were obtained for particular parametric choices [31, 32]. We have used the Krori-Barua ansatz to develop anisotropic uncharged/charged self-gravitating models and checked the impact of non-minimal fluid-geometry interaction as well as decoupling parameter on them [33]-[35].

Scientific literature has introduced numerous methodologies to tackle the challenges appear when solving Einstein/modified field equations. These approaches include employing specific equations of state, known metric components, or imposing conditions of vanishing complexity. In the domain of radial and time metric components, the Finch-Skea ansatz [36] has at-

tracted significant attention from researchers as a valuable tool for exploring anisotropic compact structures. Notably, Banerjee et al. [37] introduced a family of interior solutions analogous to the BTZ exterior by employing this metric. Their work yielded physically viable results, even in lower dimensions, demonstrating the versatility and applicability of the considered ansatz. Researchers have introduced three distinct analytic solutions to the charged field equations, verifying their adherence to stability criteria [38]. The subsequent physical analysis suggests that this analog can effectively model compact stars in the presence of Maxwell field with realistic physical properties. Various approaches, such as gravitational decoupling and considering complexity factors, have been employed to discuss self-gravitating charged or uncharged systems [39]-[41].

In this article, we formulate multiple extensions of an isotropic Finch-Skea metric to the anisotropic domain by the help of a systematic technique in the framework of modified gravity. The arrangement of this paper can be understood in the following lines. Section 2 defines some fundamentals of $f(\mathcal{R}, \mathcal{T})$ theory and determines the independent components of the field equations representing the total fluid source (perfect and newly added). We then introduce the MGD scheme in section 3 whose implementation on the field equations divides them into two distinct sets. Section 4 is devoted to the computation of an unknown triplet in the Finch-Skea solution through junction conditions. A physically relevant model must satisfy some requirements that are presented in section 5. Finally, we formulate three new anisotropic solutions alongside their graphical interpretation in section 6 and summarize our results in section 7.

2 $f(\mathcal{R}, \mathcal{T})$ Gravity

The action for $f(\mathcal{R}, \mathcal{T})$ gravity can be defined in the presence of an extra matter field as [8]

$$S = \int \sqrt{-g} \left[\frac{f(\mathcal{R}, \mathcal{T})}{16\pi} + \mathbb{L}_m + \zeta \mathbb{L}_E \right] d^4x, \quad (1)$$

where \mathbb{L}_m is the Lagrangian density of the fluid distribution and \mathbb{L}_E is the additional gravitationally coupled fluid source. Here, ζ represents the decoupling parameter that examines how the new source affects the original matter field. The modified field equations can be obtained by varying the

action (1) with respect to the metric tensor. These equations are given by

$$\mathbb{G}_{\sigma\omega} = 8\pi\mathcal{T}_{\sigma\omega}^{(\text{tot})}, \quad (2)$$

where $\mathbb{G}_{\sigma\omega}$ is called the Einstein tensor representing geometry of the structure and $\mathcal{T}_{\sigma\omega}^{(\text{tot})}$ denotes the fluid distribution comprised by the interior of that spacetime. We classify the later term into three different segments as

$$\mathcal{T}_{\sigma\omega}^{(\text{tot})} = \frac{1}{f_{\mathcal{R}}}(\mathcal{T}_{\sigma\omega} + \zeta\mathbb{E}_{\sigma\omega}) + \mathcal{T}_{\sigma\omega}^{(C)}. \quad (3)$$

Here, the first two terms on the right side are the usual and additional fluid EMTs, respectively. Also, the term $\mathcal{T}_{\sigma\omega}^{(C)}$ shows the corrections of the modified theory, defined as

$$\begin{aligned} \mathcal{T}_{\sigma\omega}^{(C)} &= \frac{1}{8\pi f_{\mathcal{R}}} \left[f_{\mathcal{T}}\mathcal{T}_{\sigma\omega} + \left\{ \frac{\mathcal{R}}{2} \left(\frac{f}{\mathcal{R}} - f_{\mathcal{R}} \right) - \mathbb{L}_m f_{\mathcal{T}} \right\} g_{\sigma\omega} \right. \\ &\quad \left. - (g_{\sigma\omega}\square - \nabla_{\sigma}\nabla_{\omega})f_{\mathcal{R}} + 2f_{\mathcal{T}}g^{\zeta\beta} \frac{\partial^2 \mathbb{L}_m}{\partial g^{\sigma\omega} \partial g^{\zeta\beta}} \right], \end{aligned} \quad (4)$$

where $f_{\mathcal{T}} = \frac{\partial f(\mathcal{R}, \mathcal{T})}{\partial \mathcal{T}}$ and $f_{\mathcal{R}} = \frac{\partial f(\mathcal{R}, \mathcal{T})}{\partial \mathcal{R}}$. Moreover, $\square \equiv \frac{1}{\sqrt{-g}}\partial_{\sigma}(g^{\sigma\omega}\sqrt{-g}\partial_{\omega})$ is the D'Alembert operator and ∇_{σ} symbolizes the covariant divergence.

It is important to mention here that there are two fluid sources in the interior of a compact geometry, one is initial (which we can call as ‘‘seed’’) source and we consider it to be the isotropic perfect fluid at some initial moment. On the other hand, the second matter source is known as extra or additional fluid that produces anisotropy in the initial (seed) source. The EMT corresponding to the isotropic fluid is defined by

$$\mathcal{T}_{\sigma\omega} = (\mu + P)\mathcal{K}_{\sigma}\mathcal{K}_{\omega} + P g_{\sigma\omega}, \quad (5)$$

where P , μ and \mathcal{K}_{σ} indicate the isotropic pressure, energy density and four-velocity, respectively. Also, the trace of Eq.(2) is obtained as

$$\mathcal{R}f_{\mathcal{R}} + 3\nabla^{\sigma}\nabla_{\sigma}f_{\mathcal{R}}2f - \mathcal{T}(f_{\mathcal{T}} + 1) - \zeta\mathbb{E} + 4f_{\mathcal{T}}\mathbb{L}_m - 2f_{\mathcal{T}}g^{\zeta\beta}g^{\sigma\omega} \frac{\partial^2 \mathbb{L}_m}{\partial g^{\zeta\beta} \partial g^{\sigma\omega}} = 0.$$

When we assume a vacuum case (i.e., $\mathcal{T} = 0$), the fluid-geometry interaction vanishes and the results of this theory reduce to $f(\mathcal{R})$ framework. Moreover, we observe some extra terms in the divergence of EMT due to such interaction, leading to the non-conservation phenomenon. This non-conservation

provides an evident for the existence of an additional force that can mathematically be expressed by

$$\begin{aligned} \nabla^\sigma \mathcal{T}_{\sigma\omega} = & \frac{f_{\mathcal{T}}}{8\pi - f_{\mathcal{T}}} \left[(\mathcal{T}_{\sigma\omega} + \Upsilon_{\sigma\omega}) \nabla^\sigma \ln f_{\mathcal{T}} - \frac{1}{2} g_{\alpha\beta} \nabla_\omega \mathcal{T}^{\alpha\beta} \right. \\ & \left. + \nabla^\sigma \left(g_{\sigma\omega} \mathbf{L}_m - 2\mathcal{T}_{\sigma\omega} - 2g^{\zeta\beta} \frac{\partial^2 \mathbf{L}_m}{\partial g^{\sigma\omega} \partial g^{\zeta\beta}} \right) - \frac{8\pi\zeta}{f_{\mathcal{T}}} \nabla^\sigma \mathbf{E}_{\sigma\omega} \right]. \end{aligned} \quad (6)$$

The self-gravitating geometry is usually divided into two regions, namely interior and exterior, and both of them are distinguished from each other at some boundary called the hypersurface (Σ). The following metric describes the interior spacetime given as

$$ds^2 = -e^{a_1} dt^2 + e^{a_2} dr^2 + r^2 (d\theta^2 + \sin^2 \theta d\phi^2), \quad (7)$$

where $a_1 = a_1(r)$ and $a_2 = a_2(r)$. The four-velocity defined in Eq.(5) now becomes in relation with the metric (7) as

$$\mathcal{K}_\sigma = -\delta_\sigma^0 e^{\frac{a_1}{2}} = (-e^{\frac{a_1}{2}}, 0, 0, 0). \quad (8)$$

To understand the physical behavior of solutions to the field equations is indispensable requirement so that it can be explored whether they represent physically realistic compact models or not. This cannot be done without taking a standard model of the considered gravity theory into account. There are several models proposed in the literature, however, we adopt the simplest one among them so that the geometric deformations can effectively be employed on the corresponding field equations. The model under consideration is given as follows

$$f(\mathcal{R}, \mathcal{T}) = f_1(\mathcal{R}) + f_2(\mathcal{T}) = \mathcal{R} + 2\xi\mathcal{T}, \quad (9)$$

where ξ symbolizes an arbitrary constant and $\mathcal{T} = -\mu + 3P$. Multiple potentials showing inflation have been adopted in this context to derive potential slow-roll parameters. It was then concluded that the resulting outcomes are consistent with the observed data only for a particular range of $\xi \in (-0.37, 1.483)$ [42]. The Tolman-Kuchowicz interior possessing anisotropic fluid distribution has also been successfully developed by using the above linear model [43]. We have utilized the same model to formulate several acceptable compact interiors through the complexity-free constraint and a linear equation of state [44, 45].

Combining $f(\mathcal{R}, \mathcal{T})$ model (9) with the general field equations (7), the non-vanishing components are calculated as

$$e^{-a_2} \left(\frac{a_2'}{r} - \frac{1}{r^2} \right) + \frac{1}{r^2} = 8\pi (\mu - \zeta E_0^0) + \xi (3\mu - P), \quad (10)$$

$$e^{-a_2} \left(\frac{1}{r^2} + \frac{a_1'}{r} \right) - \frac{1}{r^2} = 8\pi (P + \zeta E_1^1) - \xi (\mu - 3P), \quad (11)$$

$$\frac{e^{-a_2}}{4} \left[a_1'^2 - a_2' a_1' + 2a_1'' - \frac{2a_2'}{r} + \frac{2a_1'}{r} \right] = 8\pi (P + \zeta E_2^2) - \xi (\mu - 3P), \quad (12)$$

where the matter terms multiplied by ξ are the corrections of modified theory and $' = \frac{\partial}{\partial r}$. Since the spherical system now possesses two fluid sources, the Tolman-Oppenheimer-Volkoff equation (6) can be generalized as

$$\begin{aligned} \frac{dP}{dr} + \frac{a_1'}{2} (\mu + P) + \frac{\zeta a_1'}{2} (E_1^1 - E_0^0) + \zeta \frac{dE_1^1}{dr} \\ + \frac{2\zeta}{r} (E_1^1 - E_2^2) = -\frac{\xi}{4\pi - \xi} (\mu' - P'). \end{aligned} \quad (13)$$

The non-zero right hand side of the above equation makes this theory non-conserved, however, $\xi = 0$ would lead to the conservation equation. This equation is, in fact, a sum of different physical forces which help to keep a self-gravitating system in an equilibrium state. We observe that the number of unknowns in Eqs.(10)-(12) are now increased due to the involvement of components of an extra source, i.e., $(a_1, a_2, \mu, P, E_0^0, E_1^1, E_2^2)$. Therefore, a systematic approach [28] must be required to work out this under-determined system.

3 Minimal Gravitational Decoupling

Gravitational decoupling is the most advantageous technique that divides the field equations into different sets by deforming the metric components from one reference frame to another, making it easy to solve these distinct systems independently. Since we need a new reference frame in which the field equations (10)-(12) shall be transformed, we assume another line element given as follows

$$ds^2 = -e^{a_3(r)} dt^2 + \frac{1}{a_4(r)} dr^2 + r^2 (d\theta^2 + \sin^2 \theta d\phi^2). \quad (14)$$

The transformation equations are defined as

$$a_3 \rightarrow a_1 = a_3 + \zeta t_1^*, \quad a_4 \rightarrow e^{-a_2} = a_4 + \zeta t_2^*, \quad (15)$$

where t_1^* and t_2^* correspond to time and radial components, respectively. We consider MGD strategy in the current setup that allows only the transformation of g_{rr} potential whereas g_{tt} component remains the same, i.e., $t_1^* \rightarrow 0$, $t_2^* \rightarrow T^*$. Accordingly, Eq.(15) turns into

$$a_3 \rightarrow a_1 = a_3, \quad a_4 \rightarrow e^{-a_2} = a_4 + \zeta T^*, \quad (16)$$

where $T^* = T^*(r)$. While using these transformations on the field equations, we must keep in mind that the spherical symmetry is not disturbed by them. We now apply a linear mapping (16) on Eqs.(10)-(12), the first resulting set characterizing the perfect fluid source is obtained as

$$e^{-a_2} \left(\frac{a_2'}{r} - \frac{1}{r^2} \right) + \frac{1}{r^2} = 8\pi\mu + \xi(3\mu - P), \quad (17)$$

$$e^{-a_2} \left(\frac{1}{r^2} + \frac{a_1'}{r} \right) - \frac{1}{r^2} = 8\pi P - \xi(\mu - 3P), \quad (18)$$

$$\frac{e^{-a_2}}{4} \left[a_1'^2 - a_2' a_1' + 2a_1'' - \frac{2a_2'}{r} + \frac{2a_1'}{r} \right] = 8\pi P - \xi(\mu - 3P). \quad (19)$$

Since the above system represents isotropic matter source, the first two field equations can completely define the corresponding interior. Hence, Eqs.(17) and (18) produce the explicit form of the energy density and pressure as

$$\mu = \frac{e^{-a_2}}{8r^2(\xi^2 + 6\pi\xi + 8\pi^2)} [\xi r a_1' + (3\xi + 8\pi) r a_2' + 2(\xi + 4\pi)(e^{a_2} - 1)], \quad (20)$$

$$P = \frac{e^{-a_2}}{8r^2(\xi^2 + 6\pi\xi + 8\pi^2)} [(3\xi + 8\pi) r a_1' + \xi r a_2' - 2(\xi + 4\pi)(e^{a_2} - 1)]. \quad (21)$$

The second set, on the other hand, is characterizing the newly added fluid source and is given as follows

$$8\pi E_0^0 = \frac{T^{*'}}{r} + \frac{T^*}{r^2}, \quad (22)$$

$$8\pi E_1^1 = T^* \left(\frac{a_1'}{r} + \frac{1}{r^2} \right), \quad (23)$$

$$8\pi E_2^2 = \frac{T^*}{4} \left(2a_1'' + a_1'^2 + \frac{2a_1'}{r} \right) + T^{*'} \left(\frac{a_1'}{4} + \frac{1}{2r} \right). \quad (24)$$

The interesting fact of the MGD scheme is that switching energy and momentum from the original source to the seed one and vice-versa is not allowed, resulting in the conservation of both sources individually. It becomes easy for us now to solve both sets of field equations independently and then add their solutions in a particular way to get the solution of total fluid setup. In the system (20) and (21), four unknowns (μ, P, a_1, a_2) are appeared which can be tackled by making any two factors known through some constraints. On the other hand, the system (22)-(24) also engages four unknowns $(T^*, E_0^0, E_1^1, E_2^2)$, thus only one constraint is needed to obtain a unique solution. Since we consider an extra fluid setup as a source of generating anisotropy in the original perfect distribution, the matter determinants must be identified as follows

$$\tilde{\mu} = \mu - \zeta E_0^0, \quad \tilde{P}_r = P + \zeta E_1^1, \quad \tilde{P}_\perp = P + \zeta E_2^2, \quad (25)$$

along with the anisotropic factor defined by

$$\tilde{\Pi} = \tilde{P}_\perp - \tilde{P}_r = \zeta(E_2^2 - E_1^1), \quad (26)$$

verifying that extracting the impact of a new fluid source (i.e., $\zeta = 0$) again leads to the parent (isotropic) source.

4 Finch-Skea Metric and Boundary Conditions

We obtain a unique solution of Eqs.(20) and (21) in this section. It is already discussed that if we adopt two constraints or a particular metric ansatz, then the four unknowns can easily be evaluated. Since we are dealing with perfect distribution, we adopt the Finch-Skea isotropic ansatz [46] given by the metric

$$ds^2 = -\frac{1}{4}(2C_1 + C_2\sqrt{C_3}r^2)^2 dt^2 + (C_3r^2 + 1)dr^2 + r^2(d\theta^2 + \sin^2\theta d\phi^2), \quad (27)$$

where a triplet (C_1, C_2, C_3) is needed to determine so that the graphical interpretation of the proposed models in the following shall be entertained.

Their dimensions are null, $\frac{1}{\ell}$ and $\frac{1}{\ell^2}$, respectively. The metric (27) produces the energy density (20) and isotropic pressure (21) as

$$\mu = \frac{1}{4r^2(\xi + 2\pi)(\xi + 4\pi)(C_3r^2 + 1)} \times \left\{ 5\xi + (\xi + 4\pi)C_3r^2 - \frac{4\xi C_1}{C_2\sqrt{C_3r^2 + 2C_1}} - \frac{3\xi + 8\pi}{C_3r^2 + 1} + 8\pi \right\}, \quad (28)$$

$$P = \frac{-1}{4r^2(\xi + 2\pi)(\xi + 4\pi)(C_3r^2 + 1)} \times \left\{ (\xi + 4\pi)C_3r^2 + \xi \left(\frac{1}{C_3r^2 + 1} - 7 \right) + \frac{4(3\xi + 8\pi)C_1}{C_2\sqrt{C_3r^2 + 2C_1}} - 16\pi \right\}. \quad (29)$$

In order to evaluate three constants, we need an exterior metric to match with the interior spherical spacetime at the interface ($\Sigma : r = R$). Moreover, the junction conditions help to understand the complete structure of a geometrical system. The interior geometry is given in Eq.(27), however, the most suitable exterior region must be vacuum, representing by the Schwarzschild solution. It is important to note the distinctions in junction conditions between \mathbb{GR} and $f(\mathcal{R})$ theory due to the inclusion of higher-order geometric terms [47, 48]. However, in the vacuum scenario, the term \mathcal{T} in the model (9) has null contribution. Consequently, the exterior line element can be adopted similarly to that of \mathbb{GR} . We express its metric in the following

$$ds^2 = -\left(1 - \frac{2M}{r}\right)dt^2 + \left(1 - \frac{2M}{r}\right)^{-1}dr^2 + r^2(d\theta^2 + \sin^2\theta d\phi^2), \quad (30)$$

where M being the total exterior mass. We consider the metric potentials of both geometries and their derivatives to be continuous across the boundary that can mathematically be expressed as

$$g_{tt}^- \stackrel{\Sigma}{=} g_{tt}^+, \quad g_{rr}^- \stackrel{\Sigma}{=} g_{rr}^+, \quad g_{tt,r}^- \stackrel{\Sigma}{=} g_{tt,r}^+, \quad (31)$$

where plus and minus signs correspond to outer and inner regions, respectively. The above three constraints provide the following equations as

$$\frac{R - 2M}{R} = \frac{1}{4}(2C_1 + C_2\sqrt{C_3r^2})^2, \quad (32)$$

$$\frac{R}{R - 2M} = C_3r^2 + 1, \quad (33)$$

$$\frac{2M}{R^2} = C_2(2C_1\sqrt{C_3}r + C_2C_3r^3). \quad (34)$$

We simultaneously solve Eqs.(32)-(34) to get the following constants as

$$C_1 = \frac{2R - 5M}{2R\sqrt{R - 2M}}, \quad (35)$$

$$C_2 = \frac{1}{R^{\frac{3}{2}}}\sqrt{\frac{M}{2}}, \quad (36)$$

$$C_3 = \frac{2M}{R^2(R - 2M)}. \quad (37)$$

Another way to find these constants is to assume the first two constraints given in Eq.(31) along with the disappearing pressure at the spherical boundary (i.e., $P \stackrel{\Sigma}{=} 0$). These three equations would generate different values of the triplet which can also be used to perform the graphical analysis.

5 Physical Constraints on Compact Models

The literature is full of exact/numerical solutions to the field equations in GR or any other modified gravity. So the question can arise in one's mind whether all these solutions are of interest for the scientific community or not, however, the answer is no. Researchers [49, 50] provided multiple constraints that must be implemented on the compact models to check whether they are physically realistic or not. Thus, the only solutions fulfilling the following constraints are significant.

- Existing the singularity inside a compact structure is the first primary factor that demands our attention. Therefore, our investigation requires to confirm the non-singular nature of both metric components of Finch-Skea ansatz. Ensuring their increasing nature outwards is also a crucial requirement to obtain a viable self-gravitating structure. In the following, we check the behavior of time/radial components of the metric (27) at the center.

$$e^{a_1(r)}|_{r=0} = C_1^2, \quad e^{a_2(r)}|_{r=0} = 1.$$

The first derivative of these potentials is

$$(e^{a_1(r)})' = 2C_2\sqrt{C_3}r \left(\frac{1}{2}C_2\sqrt{C_3}r^2 + C_1 \right), \quad (e^{a_2(r)})' = 2C_3r,$$

and we find them zero at $r = 0$, identifying the increasing profile of both components, hence, the Finch-Skea ansatz is valid to be used.

- It is imperative to study the nature of fluid-related parameters such as pressure and energy density. These components must exhibit finite and positive values throughout the entire domain. Further, they must be maximum (or minimum) at the center (or the outer boundary $\Sigma : r = R$). Likewise, we can say that their decreasing trend towards the boundary can be guaranteed if the first derivatives of these parameters disappear at $r = 0$ while showing a negative gradient outwards.
- The spherical system possesses a mass that can be evaluated in terms of both geometry and fluid distribution. Here, we calculate the mass of the considered setup using the later definition. Its mathematical description is

$$m(r) = \frac{1}{2} \int_0^R w^2 \mu dw. \quad (38)$$

One more crucial concept in the field of astrophysics, particularly in the study of compact stars, is the compactness factor that measures the tight concentration of mass within the given region. It is also expressed as mass to the size (radius) ratio of a compact body, i.e., $\nu(r) = \frac{m(r)}{r}$. A structure having a high compactness value describes that a large amount of matter is packed into a very small volume. Such objects produce robust gravitational effects. For the case of a spherical body, the compactness has been found to be less than $\frac{4}{9}$ [46]. A self-gravitating object's surface emits light/electromagnetic radiations due to the strong gravitational effects of other near by bodies. A phenomenon that observes the change in the wavelength of those radiations is called surface redshift and we can define it in terms of the compactness as

$$z(r) = \frac{1 - \sqrt{1 - 2\nu(r)}}{\sqrt{1 - 2\nu(r)}}. \quad (39)$$

It is important to highlight that the surface redshift attains its maximum value of 5.211 in the context of anisotropic fluid distribution [51] whereas it becomes less for an isotropic configuration.

- The viability of the interior compact fluid configuration can be checked the energy conditions. They are, in fact, linear combinations of pressure

and the density reigning the isotropic/anisotropic setup. Ensuring their positive profile throughout the domain guarantees the viability of the developed model and thus the existence of usual matter is verified. If any of them is not satisfied, an exotic fluid exists. In relation with anisotropic interior, these conditions are

$$\begin{aligned} \mu &\geq 0, & \mu + P_{\perp} &\geq 0, & \mu + P_r &\geq 0, \\ \mu - P_{\perp} &\geq 0, & \mu - P_r &\geq 0, & \mu + 2P_{\perp} + P_r &\geq 0. \end{aligned} \quad (40)$$

The positive behavior of the physical determinants demands only the satisfaction of the dominant bounds (i.e., $\mu - P_r \geq 0$ and $\mu - P_{\perp} \geq 0$ implying $\mu \geq P_{\perp}$ and $\mu \geq P_r$, respectively) as all other conditions would be trivially fulfilled.

- A celestial body may possess several components due to which there occur fluctuations in its interior, departing that body from the state of hydrostatic equilibrium. This leads to the instability of the considered fluid distribution and thus the long-term existence of celestial objects may not take place. In this regard, multiple approaches based on the sound speed and perturbation methods have been suggested to analyze the structural stability. It has been found that the speed of light must be greater than the sound speed only if the body is stable. Mathematically,

$$0 < v_{sr}^2 = \frac{dP_r}{d\mu}, \quad v_{s\perp}^2 = \frac{dP_{\perp}}{d\mu} < 1,$$

where v_{sr}^2 and $v_{s\perp}^2$ are the radial and tangential speeds of sound, respectively [52]. In a similar fashion, Herrera [53] proposed that the cracking can be occurred if the total force in the radial direction changes its sign. Avoiding such cracking is necessary to obtain a physically stable model. It is found that the factor $|v_{s\perp}^2 - v_{sr}^2|$ must lie between -1 and 1 in order to avoid the cracking.

6 Some New Anisotropic Solutions

In the last couple of years, many researchers are actively involved in finding the solutions of the field equations that characterize the interior matter distribution in different theories of gravity. For this purpose, several

constraints/schemes have been suggested, resulting in physically acceptable compact celestial structures. Since we are left to solve the system (22)-(24) containing four unknowns, only one constraint is required at a time to find the corresponding unique solution. In this paper, we choose the following constraints

- Density-like constraint,
- Pressure-like constraint,
- A linear equation of state.

6.1 Model I

According to the density-like constraint, the energy density of both the matter sources can be put equal to each other [54]. This provides several anisotropic physically relevant compact interiors in \mathbb{GR} and modified theories. We define it as follows

$$\mu = E_0^0. \quad (41)$$

Substituting Eqs.(20) and (23) in the above equation, we get the linear-order differential equation given by

$$\begin{aligned} & \frac{1}{8\pi} \left\{ \frac{T^{*'}(r)}{r} + \frac{T^*(r)}{r^2} \right\} - \frac{e^{-a_2}}{8r^2(\xi^2 + 6\pi\xi + 8\pi^2)} \\ & \times [\xi r a'_1 + (3\xi + 8\pi) r a'_2 + 2(\xi + 4\pi)(e^{a_2} - 1)] = 0, \end{aligned} \quad (42)$$

that becomes after combining with the metric (27) as

$$\begin{aligned} & \frac{1}{8\pi} \left\{ \frac{T^{*'}(r)}{r} + \frac{T^*(r)}{r^2} \right\} - \frac{1}{4r^2(\xi + 2\pi)(\xi + 4\pi)(C_3 r^2 + 1)} \\ & \times \left\{ 5\xi + (\xi + 4\pi)C_3 r^2 - \frac{4\xi C_1}{C_2 \sqrt{C_3} r^2 + 2C_1} - \frac{3\xi + 8\pi}{C_3 r^2 + 1} + 8\pi \right\} = 0. \end{aligned} \quad (43)$$

This equation involves only one unknown as the deformation function, thus we can easily solve it. It is not possible sometimes to calculate the exact solutions of the differential equations due to the involvement of complex functions. However, in this case, we obtain an analytic solution successfully. The deformation function is obtained as

$$T^*(r) = \frac{\pi}{r C_3^{5/4} (\xi^2 + 6\pi\xi + 8\pi^2) (2C_1 \sqrt{C_3} - C_2)} \left[2r C_3^{5/4} (2C_1 \sqrt{C_3} - C_2) \right]$$

$$\begin{aligned}
& \times (\xi + 4\pi) + 4\sqrt{2C_1C_2}\xi C_3 \tan^{-1} \left\{ \sqrt{\frac{C_2}{2C_1}} \sqrt[4]{C_3} r \right\} + \tan^{-1} \left\{ \sqrt{C_3} r \right\} \\
& \times \xi C_3^{3/4} (2C_1\sqrt{C_3} - 5C_2) - \frac{(3\xi + 8\pi)(2C_1\sqrt{C_3} - C_2)C_3^{5/4}r}{C_3r^2 + 1} \Big] + \frac{A_1}{r},
\end{aligned} \tag{44}$$

where A_1 is the integration constant with dimension of length and we take it to be zero to obtain a non-singular solution at $r = 0$. The deformed g_{rr} metric component takes the form as

$$e^{a_2(r)} = \frac{1 + C_3r^2}{1 + \zeta T^*(1 + C_3r^2)}. \tag{45}$$

Finally, the effective physical parameters (25) are defined as

$$\begin{aligned}
\tilde{\mu} = & \frac{\sqrt{C_3}(1 - \zeta)}{4(\xi + 2\pi)(\xi + 4\pi)(C_2\sqrt{C_3}r^2 + 2C_1)(C_3r^2 + 1)^2} \left[2C_1\sqrt{C_3}\{4(\xi + 3\pi) \right. \\
& \left. + (\xi + 4\pi)C_3r^2\} + C_2\{2\xi + (\xi + 4\pi)C_3^2r^4 + 6(\xi + 2\pi)C_3r^2\} \right], \tag{46}
\end{aligned}$$

$$\begin{aligned}
\tilde{P}_r = & \frac{-1}{8C_3^{5/4}r^2(\xi + 2\pi)(\xi + 4\pi)(C_2 - 2C_1\sqrt{C_3})(C_3r^2 + 1)} \left[\zeta r(C_3r^2 + 1) \right. \\
& \times \left(\frac{4\sqrt{C_3}C_2}{C_2\sqrt{C_3}r^2 + 2C_1} + \frac{1}{r^2} \right) \left\{ \frac{(3\xi + 8\pi)(C_2 - 2C_1\sqrt{C_3})C_3^{5/4}r}{C_3r^2 + 1} - 2(\xi + 4\pi) \right. \\
& \times (C_2 - 2C_1\sqrt{C_3})C_3^{5/4}r + 4\sqrt{2}\xi\sqrt{C_1}\sqrt{C_2}C_3 \tan^{-1} \left(\frac{\sqrt{C_2}\sqrt[4]{C_3}r}{\sqrt{2}\sqrt{C_1}} \right) + C_3^{3/4} \\
& \left. \times \xi(2C_1\sqrt{C_3} - 5C_2) \tan^{-1}(\sqrt{C_3}r) \right\} + 2(C_2 - 2C_1\sqrt{C_3})C_3^{5/4} \left\{ (\xi + 4\pi) \right. \\
& \left. \times C_3r^2 + \xi \left(\frac{1}{C_3r^2 + 1} - 7 \right) + \frac{4(3\xi + 8\pi)C_1}{C_2\sqrt{C_3}r^2 + 2C_1} - 16\pi \right\} \Big], \tag{47}
\end{aligned}$$

$$\begin{aligned}
\tilde{P}_\perp = & \frac{-1}{8C_3^{5/4}r^2(\xi + 2\pi)(\xi + 4\pi)(C_2 - 2C_1\sqrt{C_3})(C_3r^2 + 1)} \left[\zeta r(C_3r^2 + 1) \right. \\
& \times \left(\frac{4C_3C_2^2r^2}{(C_2\sqrt{C_3}r^2 + 2C_1)^2} + \frac{2\sqrt{C_3}C_2}{C_2\sqrt{C_3}r^2 + 2C_1} + \frac{4C_1C_2\sqrt{C_3} - 2C_2^2C_3r^2}{(C_3^{3/2}r^2 + 2C_1)^2} \right) \\
& \left. \times \left\{ \frac{(3\xi + 8\pi)(C_2 - 2C_1\sqrt{C_3})C_3^{5/4}r}{C_3r^2 + 1} + 2(\xi + 4\pi)(2C_1\sqrt{C_3} - C_2)C_3^{5/4}r \right. \right.
\end{aligned}$$

$$\begin{aligned}
& + 4\sqrt{2}\xi\sqrt{C_1}\sqrt{C_2}C_3 \tan^{-1} \left(\frac{\sqrt{C_2}\sqrt[4]{C_3}r}{\sqrt{2}\sqrt{C_1}} \right) + \xi(2C_1\sqrt{C_3} - 5C_2)C_3^{3/4} \\
& \times \tan^{-1}(\sqrt{C_3}r) \left. \right\} + 2(C_2 - 2C_1\sqrt{C_3})C_3^{5/4} \left\{ \xi \left(\frac{1}{C_3r^2 + 1} - 7 \right) + C_3r^2 \right. \\
& \times (\xi + 4\pi) + \frac{4(3\xi + 8\pi)C_1}{C_2\sqrt{C_3}r^2 + 2C_1} - 16\pi \left. \right\} + C_3^{5/4}\zeta \left(\frac{\sqrt{C_3}C_2r}{C_2\sqrt{C_3}r^2 + 2C_1} + \frac{1}{2r} \right) \\
& \times (C_3r^2 + 1) \left\{ C_2 \left(\frac{5\xi \tan^{-1}(\sqrt{C_3}r)}{\sqrt{C_3}} - \frac{5\xi r}{C_3r^2 + 1} - \frac{2(3\xi + 8\pi)C_3r^3}{(C_3r^2 + 1)^2} \right) \right. \\
& + C_1 \left(\frac{8\xi C_2r}{C_2\sqrt{C_3}r^2 + 2C_1} - 2\xi \tan^{-1}(\sqrt{C_3}r) + \frac{4(3\xi + 8\pi)C_3^{3/2}r^3}{(C_3r^2 + 1)^2} \right. \\
& \left. \left. + \frac{2\xi\sqrt{C_3}r}{C_3r^2 + 1} \right) - \frac{4\sqrt{2}\xi\sqrt{C_1}\sqrt{C_2} \tan^{-1} \left(\frac{\sqrt{C_2}\sqrt[4]{C_3}r}{\sqrt{2}\sqrt{C_1}} \right)}{\sqrt[4]{C_3}} \right\}. \tag{48}
\end{aligned}$$

We can obtain the corresponding anisotropy by combining Eqs.(26), (47) and (48).

The graphical interpretation for this solution is given by choosing the estimated data such as the mass $M = 1.04 \pm 0.09M_\odot$ and radius $R = 8.301 \pm 0.2km$ of a star LMC X-4 [55]. As far the parametric values are concerned, we adopt the decoupling and model parameters as $\zeta = 0.1, 0.2, 0.3$ and $\xi = 0.25, 0.5, 0.75, 1$, respectively to observe the profile of the matter sector, deformed metric potential, mass, anisotropy and energy bounds for the above resulted solution. A large body of literature exists [56]-[60], indicating that the parameter ξ must assume negative values in order to guarantee hydrostatic equilibrium of stellar configurations. In this regard, we consider both values of the model parameter to check its impact on physical properties of the considered compact star. The energy density remains positive for both positive and negative values of ξ . However, the graph of the radial pressure becomes problematic because it takes negative values near the spherical boundary. Hence, we assume only positive values of this parameter to graphically interpret the solutions. The function (44) is independent of the decoupling parameter, however, the left plot of Figure 1 shows that it possesses increasing trend outwards for all values of ξ . The g_{rr} component (45) is also plotted in the same Figure that starts from 1 and shows increasing behavior.

The effective matter determinants (46)-(48) and the anisotropic factor corresponding to the density-like constraint are plotted in Figure 2. We find

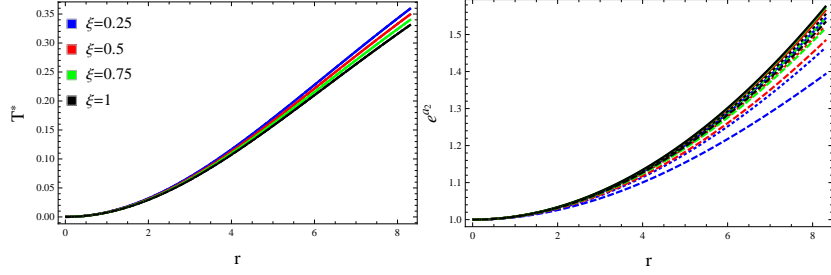


Figure 1: Deformation function (T^*) (44) and extended component (e^{a_2}) (45) for $\zeta = 0.1$ (solid), 0.2 (dotted) and 0.3 (dashed) corresponding to model I.

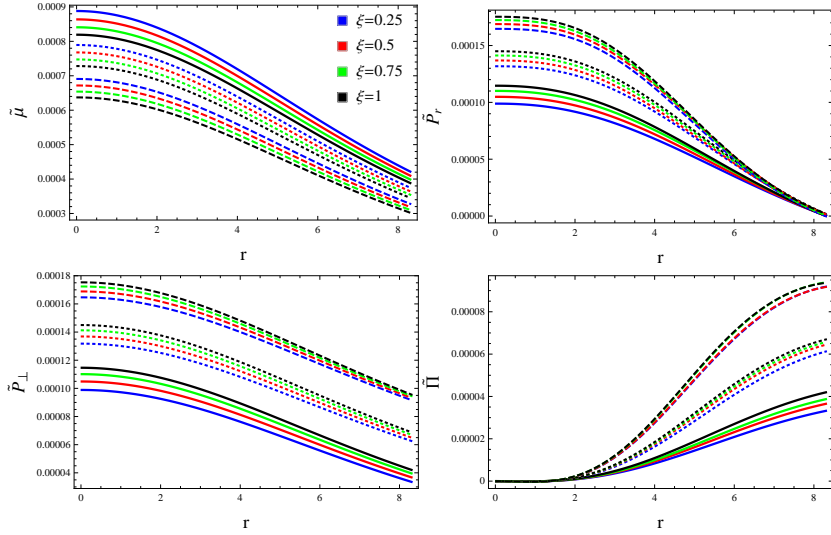


Figure 2: Effective energy density ($\tilde{\mu}$), radial pressure (\tilde{P}_r), tangential pressure (\tilde{P}_\perp) and Anisotropy ($\tilde{\Pi}$) for $\zeta = 0.1$ (solid), 0.2 (dotted) and 0.3 (dashed) corresponding to model I.

that the increment in both ζ and ξ results in decrement in the energy density. However, the radial/transverse pressures exhibit a completely opposite behavior for these parametric values. The last plot of Figure 2 indicates the null anisotropy at the center of a considered candidate while increasing outwards. We deduce that the larger values of parameters produce stronger anisotropy in the self-gravitating interior, i.e., maximum anisotropy at the surface is achieved for $\zeta = 0.3$ and $\xi = 1$. Tables 1-3 suggest the values of these parameters, fulfilling the required range for the existence of dense compact objects. Figure 3 exhibits the mass function that is found to be an increasing function from $0 < r < R$. Also, the structure becomes more dense for lower values of parameters. The plots of compactness and surface redshift indicate lower values than their proposed upper bounds. Figures 4 and 5 display the dominant energy bounds and stability criteria. It is found that the model I is viable and stable for every parametric value of ξ and ζ .

Table 1: Values of some physical parameters for $\zeta = 0.1$ corresponding to Model I.

ξ	0.25	0.5	0.75	1
μ_c (gm/cm^3)	1.1863×10^{15}	1.1551×10^{15}	1.1245×10^{15}	1.0956×10^{15}
μ_s (gm/cm^3)	5.6551×10^{14}	5.4865×10^{14}	5.3393×10^{14}	5.1841×10^{14}
P_c ($dyne/cm^2$)	1.1893×10^{35}	1.2505×10^{35}	1.3239×10^{35}	1.3852×10^{35}
ν_s	0.197	0.188	0.184	0.179
z_s	0.279	0.267	0.258	0.247

Table 2: Values of some physical parameters for $\zeta = 0.2$ corresponding to Model I.

ξ	0.25	0.5	0.75	1
μ_c (gm/cm^3)	1.0578×10^{15}	1.0268×10^{15}	1.0026×10^{15}	9.7381×10^{14}
μ_s (gm/cm^3)	5.0477×10^{14}	4.8818×10^{14}	4.7467×10^{14}	4.6704×10^{14}
P_c ($dyne/cm^2$)	1.5799×10^{35}	1.6533×10^{35}	1.6954×10^{35}	1.7399×10^{35}
ν_s	0.172	0.166	0.161	0.157
z_s	0.232	0.227	0.217	0.212

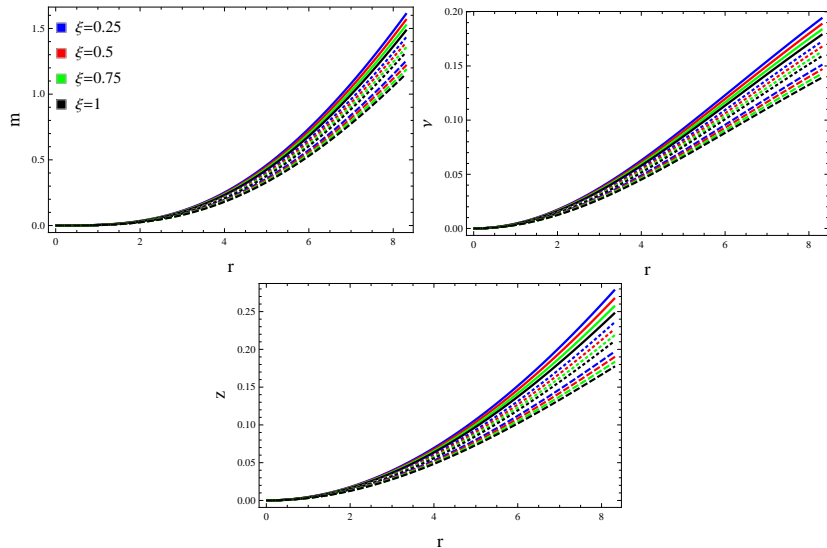


Figure 3: Mass (m), compactness (ν) and surface redshift (z) for $\zeta = 0.1$ (solid), 0.2 (dotted) and 0.3 (dashed) corresponding to model I.

Table 3: Values of some physical parameters for $\zeta = 0.3$ corresponding to Model I.

ξ	0.25	0.5	0.75	1
μ_c (gm/cm^3)	9.2244×10^{14}	8.9809×10^{14}	8.7428×10^{14}	8.4913×10^{14}
μ_s (gm/cm^3)	4.3895×10^{14}	4.2691×10^{14}	4.1767×10^{14}	4.0429×10^{14}
P_c ($dyne/cm^2$)	1.9719×10^{35}	2.0333×10^{35}	2.0694×10^{35}	2.1066×10^{35}
ν_s	0.149	0.145	0.142	0.139
z_s	0.197	0.192	0.181	0.175

6.2 Model II

This subsection adopts a pressure-like constraint [61] that equals the pressures of both parent and additional fluid sources to construct the solution of the system (22)-(24). This is widely adopted constraint in the literature in order to extend the solutions from isotropic to the anisotropic domain. The mathematical expression for this constraint is

$$P = E_1^1. \quad (49)$$

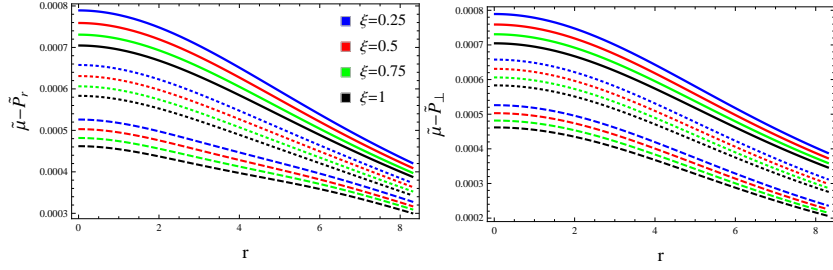


Figure 4: Energy bounds ($\tilde{\mu} - \tilde{P}_r$ and $\tilde{\mu} - \tilde{P}_\perp$) for $\zeta = 0.1$ (solid), 0.2 (dotted) and 0.3 (dashed) corresponding to model I.

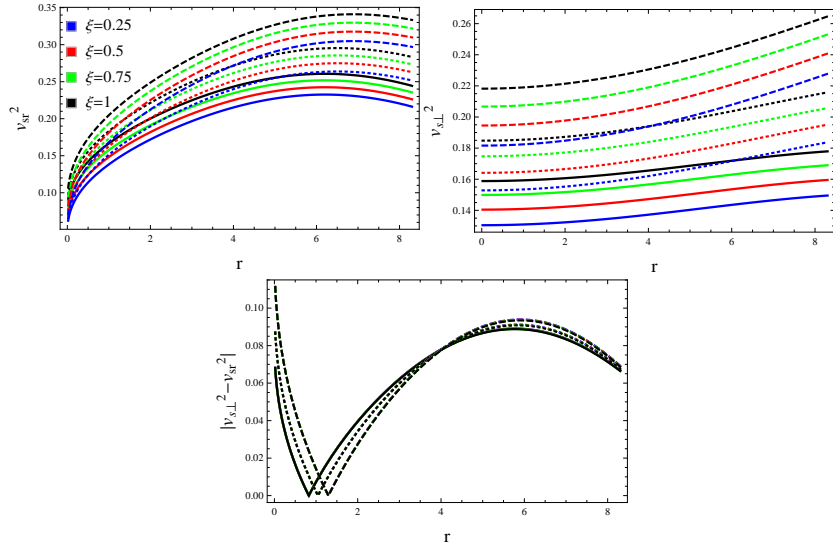


Figure 5: Radial (v_{sr}^2), tangential ($v_{s\perp}^2$) sound speeds and cracking ($|v_{s\perp}^2 - v_{sr}^2|$) for $\zeta = 0.1$ (solid), 0.2 (dotted) and 0.3 (dashed) corresponding to model I.

Equation (49) yields after joining with (21) and (24) as

$$\begin{aligned} & \frac{T^*(r)}{8\pi} \left\{ \frac{a'_1}{r} + \frac{1}{r^2} \right\} - \frac{e^{-a_2}}{8r^2(\xi^2 + 6\pi\xi + 8\pi^2)} \\ & \times [(3\xi + 8\pi)ra'_1 + \xi ra'_2 - 2(\xi + 4\pi)(e^{a_2} - 1)] = 0, \end{aligned} \quad (50)$$

that becomes in relation with the metric (27)

$$\begin{aligned} & \left(\frac{4\sqrt{C_3}C_2}{C_2\sqrt{C_3}r^2 + 2C_1} + \frac{1}{r^2} \right) T^*(r) + \frac{2\pi}{(\xi + 2\pi)(\xi + 4\pi)r^2(C_3r^2 + 1)} \\ & \times \left\{ (\xi + 4\pi)C_3r^2 + \xi \left(\frac{1}{C_3r^2 + 1} - 7 \right) + \frac{4(3\xi + 8\pi)C_1}{C_2\sqrt{C_3}r^2 + 2C_1} - 16\pi \right\} = 0, \end{aligned} \quad (51)$$

providing the deformation function as follows

$$\begin{aligned} T^*(r) = & \frac{2\pi\sqrt{C_3}r^2}{(\xi + 2\pi)(\xi + 4\pi)(5C_2\sqrt{C_3}r^2 + 2C_1)(C_3r^2 + 1)^2} \left[C_2\{2(3\xi + 8\pi) \right. \\ & \left. - (\xi + 4\pi)C_3^2r^4 + 6(\xi + 2\pi)C_3r^2\} - 2C_1\sqrt{C_3}\{(\xi + 4\pi)C_3r^2 + 4\pi\} \right]. \end{aligned} \quad (52)$$

The deformed g_{rr} component for the constraint (49) becomes

$$\begin{aligned} e^{a_2(r)} = & [(\xi + 2\pi)(\xi + 4\pi)(5C_2\sqrt{C_3}r^2 + 2C_1)(C_3r^2 + 1)^2][(\xi + 2\pi)(\xi + 4\pi) \\ & \times (5C_2\sqrt{C_3}r^2 + 2C_1)(C_3r^2 + 1) + 2\pi\sqrt{C_3}\zeta r^2\{C_2(6\xi - (\xi + 4\pi)C_3^2r^4 \\ & + 6(\xi + 2\pi)C_3r^2 + 16\pi) - 2C_1\sqrt{C_3}((\xi + 4\pi)C_3r^2 + 4\pi)\}]^{-1}. \end{aligned} \quad (53)$$

Hence, the effective energy density, pressure components (25) and anisotropy (26) are given by

$$\begin{aligned} \tilde{\mu} = & \frac{\sqrt{C_3}}{4(\xi + 2\pi)(\xi + 4\pi)(C_2\sqrt{C_3}r^2 + 2C_1)(5C_2\sqrt{C_3}r^2 + 2C_1)^2(C_3r^2 + 1)^3} \\ & \times \left[2C_1C_2^2\sqrt{C_3}r^2\{20\xi - 16(3\xi + 8\pi)\zeta + C_3r^2(12(\xi(15 - 2\zeta) + (3\zeta + 35) \right. \\ & \times \pi) + C_3r^2(\xi(71\zeta + 195) + (\xi + 4\pi)C_3(3\zeta + 35)r^2 + 16\pi(11\zeta + 35)))\} \\ & \left. + 8C_1^3\sqrt{C_3}\{4(\xi + 3\pi(\zeta + 1)) + C_3(\zeta + 1)r^2(5\xi + (\xi + 4\pi)C_3r^2 + 16\pi)\} \right] \end{aligned}$$

$$\begin{aligned}
& - 4C_1^2 C_2 \{ 2\xi(9\zeta - 1) + C_3 r^2 (12(2\xi(\zeta - 2) + \pi(\zeta - 11)) + C_3 r^2 (-3\xi \\
& \times (7\zeta + 19) + (\xi + 4\pi)C_3(\zeta - 11)r^2 - 16\pi(2\zeta + 11))) + 48\pi\zeta \} + 5C_2^3 C_3 \\
& \times r^4 \{ C_3 r^2 (40\xi + C_3 r^2 (\xi(11\zeta + 35) + (\xi + 4\pi)C_3(\zeta + 5)r^2 + 16\pi(2\zeta + 5)) \\
& + 12\pi(\zeta + 5)) - 2(\xi(3\zeta - 5) + 8\pi\zeta) \} \Big], \quad (54)
\end{aligned}$$

$$\begin{aligned}
\tilde{P}_r = & \frac{-\sqrt{C_3}(\zeta + 1)}{4(\xi + 2\pi)(\xi + 4\pi)(C_2\sqrt{C_3}r^2 + 2C_1)(C_3r^2 + 1)^2} \left[2C_1\sqrt{C_3} \{ 4\pi + C_3r^2 \right. \\
& \left. \times (\xi + 4\pi) \} + C_2 \{ (\xi + 4\pi)C_3^2 r^4 - 2(3\xi + 8\pi) - 6(\xi + 2\pi)C_3r^2 \} \right], \quad (55)
\end{aligned}$$

$$\begin{aligned}
\tilde{P}_1 = & \frac{-\sqrt{C_3}}{4(\xi + 2\pi)(\xi + 4\pi)(C_2\sqrt{C_3}r^2 + 2C_1)(5C_2\sqrt{C_3}r^2 + 2C_1)^2(C_3r^2 + 1)^3} \\
& \times \left[2C_1C_2^2\sqrt{C_3}r^2 \{ C_3r^2(C_3r^2(64\xi\zeta - 25\xi + (\xi + 4\pi)C_3(12\zeta + 35)r^2 \right. \\
& + 204\pi\zeta + 120\pi) - 4(9\xi\zeta + 30\xi - 11\pi\zeta + 45\pi)) - (3\xi + 8\pi)(7\zeta + 10) \\
& \times 2 \} + 8C_1^3\sqrt{C_3} \{ C_3r^2(2\xi\zeta + \xi + (\xi + 4\pi)C_3r^2 + 4\pi(\zeta + 2)) + \pi(\zeta + 1) \\
& \times 4 \} + 4C_1^2C_2 \{ C_3r^2(2(2\pi(5\zeta + 3) - 3\xi(\zeta + 2)) + C_3r^2(\xi(18\zeta + 5) + 11 \\
& \times (\xi + 4\pi)C_3r^2 + 36\pi(\zeta + 2))) - 2(3\xi + 8\pi)(\zeta + 1) \} + 5C_2^3C_3r^4 \{ C_3r^2 \\
& \times (C_3r^2(4(\xi + 7\pi)\zeta - 5(5\xi + 8\pi) + (\xi + 4\pi)C_3(4\zeta + 5)r^2) - 2((\zeta + 2) \\
& \times 15\xi + \pi(26\zeta + 70))) - 2(3\xi + 8\pi)(4\zeta + 5) \} \Big], \quad (56)
\end{aligned}$$

$$\begin{aligned}
\tilde{\Pi} = & \frac{\zeta r^2 C_3}{4(\xi + 2\pi)(\xi + 4\pi)(C_2\sqrt{C_3}r^2 + 2C_1)(5C_2\sqrt{C_3}r^2 + 2C_1)^2(C_3r^2 + 1)^3} \\
& \times \left[8C_3C_1^3((\xi + 4\pi)C_3r^2 - \xi + 4\pi) + 4C_2\sqrt{C_3}C_1^2(C_3r^2(11(\xi + 4\pi)C_3r^2 \right. \\
& + 36\pi - 13\xi) - 6\xi - 8\pi) + 2C_2^2C_1(C_3r^2(C_3r^2(23(\xi + 4\pi)C_3r^2 - 89\xi \\
& - 84\pi) - 28(3\xi + 8\pi)) - 6(3\xi + 8\pi)) + 5C_2^3\sqrt{C_3}r^2(C_3r^2(C_3r^2(C_3r^2 \\
& \times (\xi + 4\pi) - 29\xi - 68\pi) - 30\xi - 88\pi) - 2(3\xi + 8\pi)) \Big]. \quad (57)
\end{aligned}$$

The behavior of the deformation function (52) is shown in the left plot of Figure 6 that becomes null at the center, increases up to $r \approx 5.5$ and then again decreases towards the boundary. The same Figure also exhibits

the extended radial component (53), presenting an acceptable (increasing) behavior throughout. The desired behavior (already discussed in section 5) of the effective energy density and both pressure components (54)-(56) are observed in Figure 7, thus they reign the interior of a compact object. The behavior of such effective parameters in relation with ξ and ζ are found the same as for the model I. Tables 4-6 present their values for all choices of these parameters which are in accordance with the observed data for compact stars. The vanishing radial pressure at $r = R = 8.301$ confirms the continuity of the second fundamental form of the matching conditions. Moreover, there does not exist pressure anisotropy at the center that initially decreases outwards and then again increases towards the spherical junction (lower right plot of Figure 7).

Table 4: Values of some physical parameters for $\zeta = 0.1$ corresponding to Model II.

ξ	0.25	0.5	0.75	1
μ_c (gm/cm^3)	1.2897×10^{15}	1.2542×10^{15}	1.2177×10^{15}	1.1832×10^{15}
μ_s (gm/cm^3)	6.2571×10^{14}	6.1006×10^{14}	5.9253×10^{14}	5.7701×10^{14}
P_c ($dyne/cm^2$)	8.7187×10^{34}	9.6266×10^{34}	1.0427×10^{35}	1.1133×10^{35}
ν_s	0.188	0.184	0.178	0.173
z_s	0.267	0.256	0.246	0.238

Table 5: Values of some physical parameters for $\zeta = 0.2$ corresponding to Model II.

ξ	0.25	0.5	0.75	1
μ_c (gm/cm^3)	1.2669×10^{15}	1.2249×10^{15}	1.1868×10^{15}	1.1496×10^{15}
μ_s (gm/cm^3)	6.4149×10^{14}	6.2624×10^{14}	6.0349×10^{14}	5.9052×10^{14}
P_c ($dyne/cm^2$)	9.5087×10^{34}	1.0501×10^{35}	1.1376×10^{35}	1.2144×10^{35}
ν_s	0.188	0.182	0.176	0.172
z_s	0.266	0.255	0.245	0.236

Table 6: Values of some physical parameters for $\zeta = 0.3$ corresponding to Model II.

ξ	0.25	0.5	0.75	1
μ_c (gm/cm^3)	1.2404×10^{15}	1.1941×10^{15}	1.1544×10^{15}	1.1159×10^{15}
μ_s (gm/cm^3)	6.3909×10^{14}	6.1728×10^{14}	6.0082×10^{14}	5.8397×10^{14}
P_c ($dyne/cm^2$)	1.0305×10^{35}	1.1376×10^{35}	1.2325×10^{35}	1.3239×10^{35}
ν_s	0.187	0.183	0.177	0.171
z_s	0.267	0.255	0.243	0.235

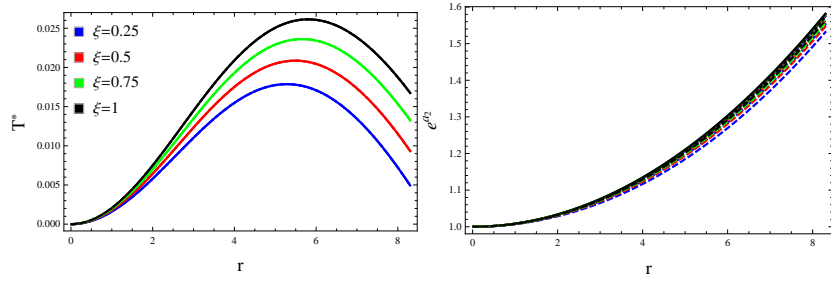


Figure 6: Deformation function (T^*) (52) and extended component (e^{a2}) (53) for $\zeta = 0.1$ (solid), 0.2 (dotted) and 0.3 (dashed) corresponding to model II.

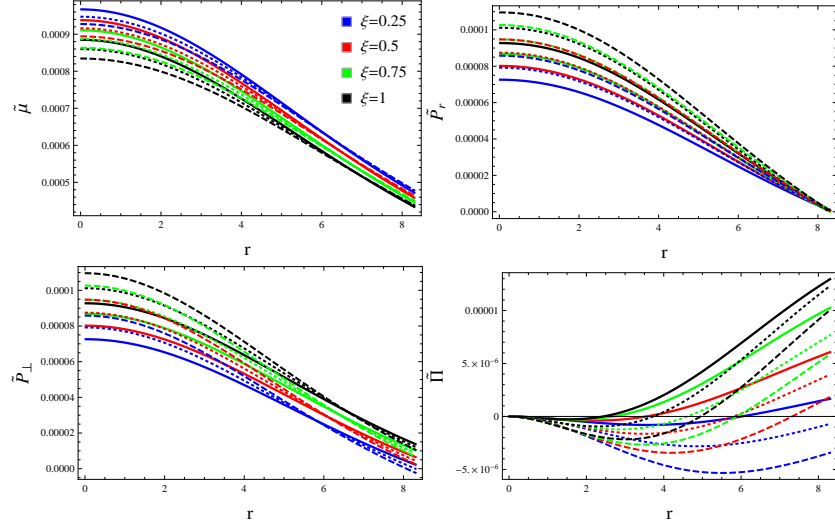


Figure 7: Effective energy density ($\tilde{\mu}$), radial pressure (\tilde{P}_r), tangential pressure (\tilde{P}_\perp) and Anisotropy ($\tilde{\Pi}$) for $\zeta = 0.1$ (solid), 0.2 (dotted) and 0.3 (dashed) corresponding to model II.

The calculated mass of a star LMC X-4 for our developed model II is exhibited in Figure 8 which is consistent with the observed mass. The other two plots of this Figure indicate an admissible behavior of the surface redshift and compactness. Two energy bounds such as $\tilde{\mu} - \tilde{P}_r \geq 0$ and $\tilde{\mu} - \tilde{P}_\perp \geq 0$ are pictured in Figure 9 whose acceptable profile shows the viability of our solution. Hence, the usual matter exists in the proposed interior. Finally, Figure 10 tests the stability criteria and all three plots confirm that our model II is stable for all parametric choices.

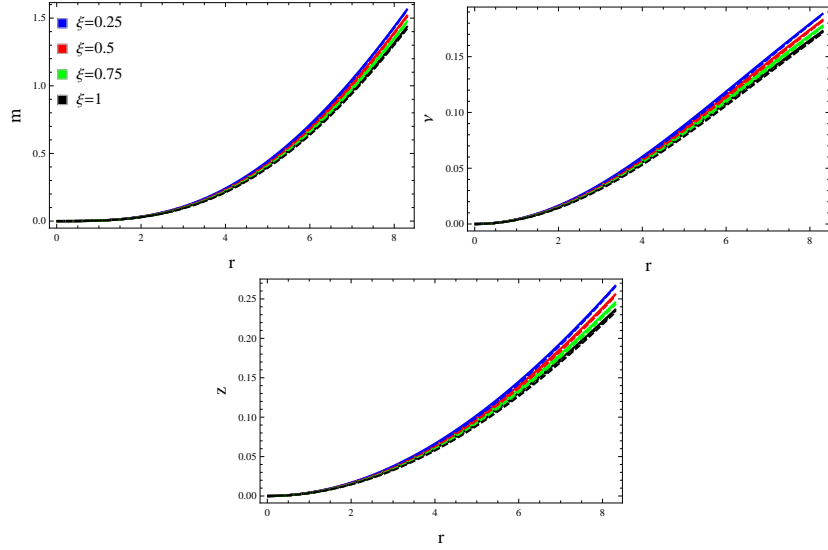


Figure 8: Mass (m), compactness (ν) and surface redshift (z) for $\zeta = 0.1$ (solid), 0.2 (dotted) and 0.3 (dashed) corresponding to model II.

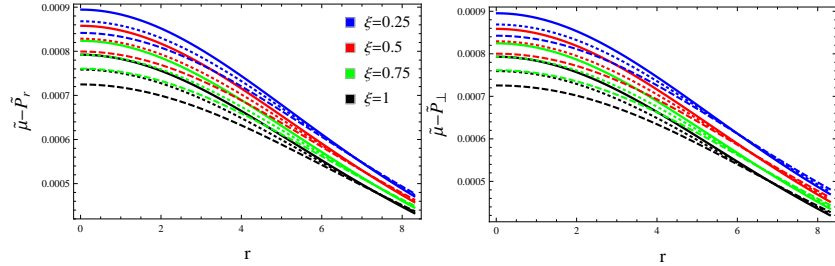


Figure 9: Energy bounds ($\tilde{\mu} - \tilde{P}_r$ and $\tilde{\mu} - \tilde{P}_\perp$) for $\zeta = 0.1$ (solid), 0.2 (dotted) and 0.3 (dashed) corresponding to model II.

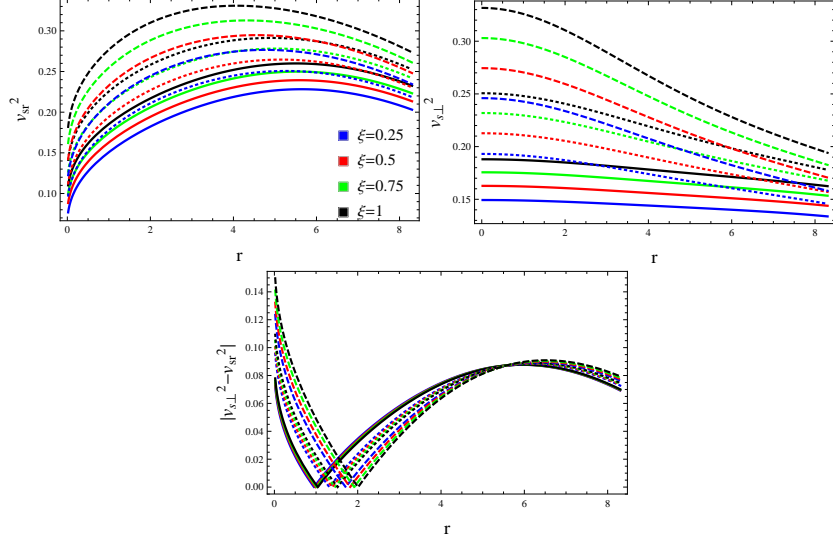


Figure 10: Radial (v_{sr}^2), tangential ($v_{s\perp}^2$) sound speeds and cracking ($|v_{s\perp}^2 - v_{sr}^2|$) for $\zeta = 0.1$ (solid), 0.2 (dotted) and 0.3 (dashed) corresponding to model II.

6.3 Model III

Here, we adopt a linear equation of state [62] that interlinks the matter sector of the additional fluid source as another constraint so that a unique solution of the system (22)-(24) is obtained. This equation of state is given as follows

$$E_1^1(r) = \kappa_1 E_0^0(r) + \kappa_2, \quad (58)$$

where κ_1 and κ_2 are arbitrary constants whose different values may intensely affect the calculated solution. Joining Eqs.(23), (24) and (58) together, we get the following linear-order different equation

$$\frac{\kappa_1 T^{*'}(r)}{r} - \left(\frac{a_1'}{r} + \frac{1}{r^2} - \frac{\kappa_1}{r^2} \right) T^*(r) + 8\pi\kappa_2 = 0. \quad (59)$$

Note that the third component of an extra fluid configuration (E_2^2) can also be involved in the constraint (58), however, the resulting second-order differential equation becomes more complicated and may not be solved. When we substitute the metric (27) in (59), the differential equation takes the form

$$T^*(r) \left\{ \frac{4\sqrt{C_3}C_2}{C_2\sqrt{C_3}r^2 + 2C_1} - \frac{\kappa_1}{r^2} + \frac{1}{r^2} \right\} - \frac{\kappa_1 T^{*'}(r)}{r} - 8\pi\kappa_2 = 0. \quad (60)$$

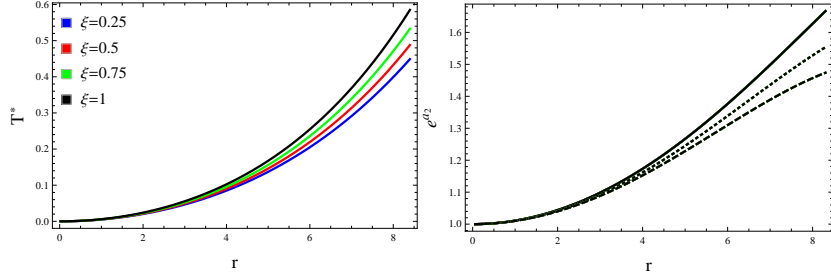


Figure 11: Deformation function (T^*) and extended component (e^{a_2}) for $\zeta = 0.1$ (solid), 0.2 (dotted) and 0.3 (dashed) corresponding to model III.

Since the above equation is linear in $T^*(r)$, we firstly solve it through exact integration and obtain the deformation function in terms of hypergeometric terms. We face difficulty while plotting the corresponding physical factors due to such complex terms. We, therefore, apply the numerical integration to solve Eq.(60) for $T^*(r)$ by providing the initial condition $T^*(r)|_{r=0} = 0$ along with $\kappa_1 = 1.1$ and $\kappa_2 = 0.01$. Figure 11 shows the variation of the deformation function with respect to ξ that possesses an increasing profile for $0 < r < R$. The right plot of the same Figure indicates that the impact of ξ on the extended g_{rr} component is negligible due to the constraint (58) that solely depends on the additional sector. However, it exhibits increasing trend for every value of ζ . Further, the matter triplet and anisotropy are obtained through Eqs.(25) and (26) and are plotted in Figure 12. We observe that the energy density and both pressures show opposite trend with respect to ζ and ξ at the center.

Tables 7-9 present the numerical values of these physical quantities, clarifying the effect of both parameters. The increasing trend of anisotropic factor provides an outward force that may help to maintain the stability of our model III. Figure 13 shows that the mass function is increasing outwards and the proposed model is more dense for $\xi = 0.25$ and $\zeta = 0.1$. The other two factors in this Figure are found within the allowable limits. Figure 14 demonstrates that there must exist usual matter in the interior because the dominant energy conditions are fulfilled. The stability analysis is shown in Figure 15 from which we deduce that our model III is stable only for $\zeta = 0.1$ and 0.2 . However, the tangential sound speed criterion is not satisfied for $\zeta = 0.3$.

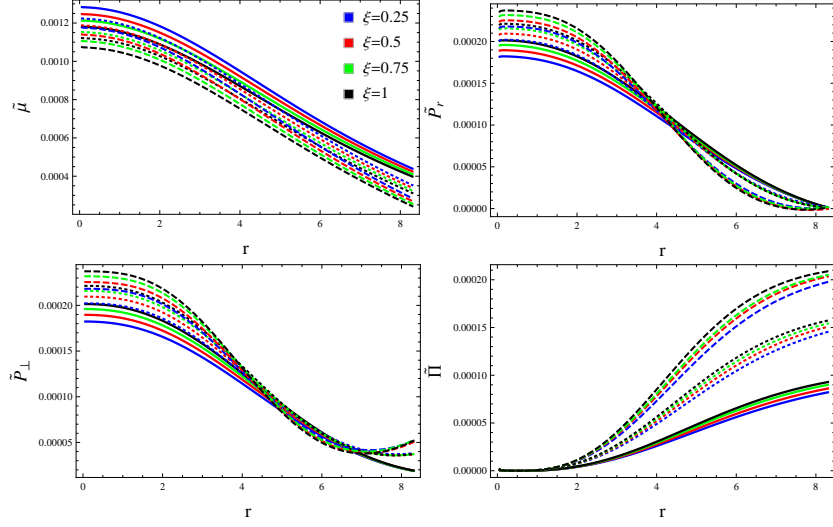


Figure 12: Effective energy density ($\tilde{\mu}$), radial pressure (\tilde{P}_r), tangential pressure (\tilde{P}_\perp) and Anisotropy ($\tilde{\Pi}$) for $\zeta = 0.1$ (solid), 0.2 (dotted) and 0.3 (dashed) corresponding to model III.

Table 7: Values of some physical parameters for $\zeta = 0.1$ corresponding to Model III.

ξ	0.25	0.5	0.75	1
μ_c (gm/cm^3)	1.7164×10^{15}	1.6669×10^{15}	1.6215×10^{15}	1.5746×10^{15}
μ_s (gm/cm^3)	5.9106×10^{14}	5.6898×10^{14}	5.4196×10^{14}	5.2992×10^{14}
P_c ($dyne/cm^2$)	2.1884×10^{35}	2.2629×10^{35}	2.3639×10^{35}	2.4169×10^{35}
ν_s	0.195	0.189	0.183	0.178
z_s	0.279	0.267	0.255	0.246

Table 8: Values of some physical parameters for $\zeta = 0.2$ corresponding to Model III.

ξ	0.25	0.5	0.75	1
μ_c (gm/cm^3)	1.6375×10^{15}	1.5853×10^{15}	1.5425×10^{15}	1.4944×10^{15}
μ_s (gm/cm^3)	4.7145×10^{14}	4.5152×10^{14}	4.3547×10^{14}	4.0978×10^{14}
P_c ($dyne/cm^2$)	2.4277×10^{35}	2.5143×10^{35}	2.5901×10^{35}	2.6561×10^{35}
ν_s	0.171	0.165	0.161	0.154
z_s	0.235	0.224	0.214	0.204

Table 9: Values of some physical parameters for $\zeta = 0.3$ corresponding to Model III.

ξ	0.25	0.5	0.75	1
μ_c (gm/cm^3)	1.5719×10^{15}	1.5251×10^{15}	1.4797×10^{15}	1.4302×10^{15}
μ_s (gm/cm^3)	3.8169×10^{14}	3.6162×10^{14}	3.4168×10^{14}	3.1961×10^{14}
P_c ($dyne/cm^2$)	2.6177×10^{35}	2.7054×10^{35}	2.7981×10^{35}	2.8809×10^{35}
ν_s	0.153	0.148	0.142	0.137
z_s	0.203	0.192	0.183	0.175

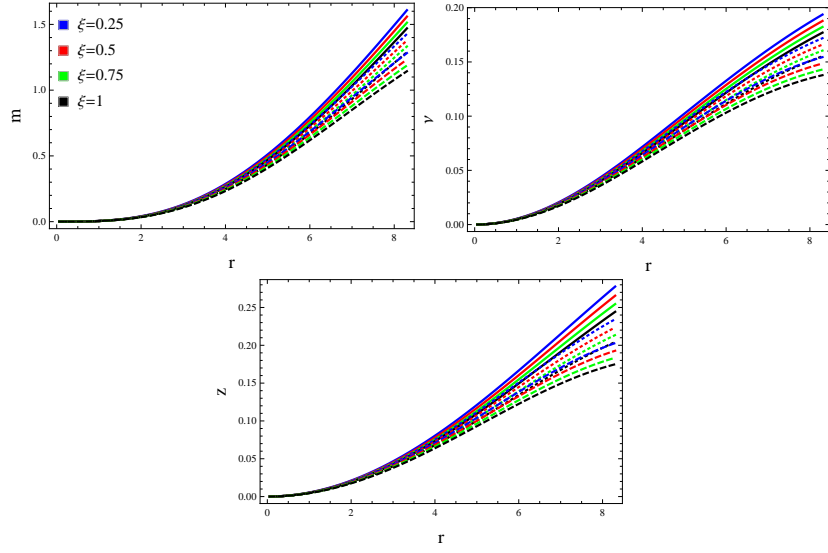


Figure 13: Mass (m), compactness (ν) and surface redshift (z) for $\zeta = 0.1$ (solid), 0.2 (dotted) and 0.3 (dashed) corresponding to model III.

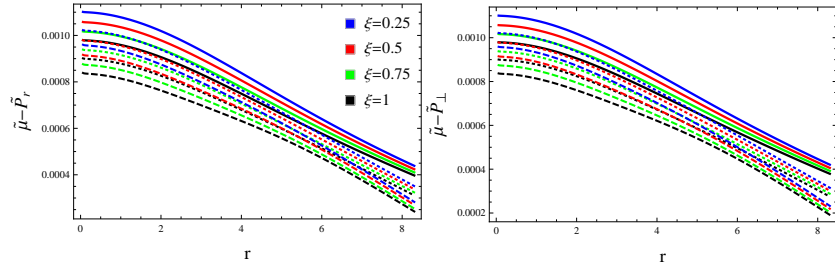


Figure 14: Energy bounds ($\tilde{\mu} - \tilde{P}_r$ and $\tilde{\mu} - \tilde{P}_\perp$) for $\zeta = 0.1$ (solid), 0.2 (dotted) and 0.3 (dashed) corresponding to model III.

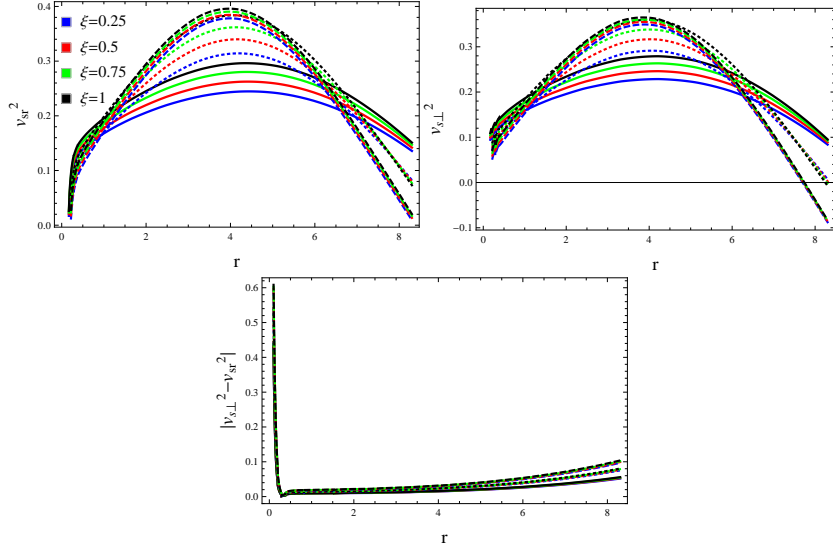


Figure 15: Radial (v_{sr}^2), tangential ($v_{s\perp}^2$) sound speeds and cracking ($|v_{s\perp}^2 - v_{sr}^2|$) for $\zeta = 0.1$ (solid), 0.2 (dotted) and 0.3 (dashed) corresponding to model III.

7 Conclusions

This paper is devoted to the formulation of three different extensions of an isotropic Finch-Skea metric to the anisotropic domain with the help of the MGD technique in a modified linear $f(\mathcal{R}, \mathcal{T}) = \mathcal{R} + 2\xi\mathcal{T}$ theory. In order to address this, a static spherical geometry has been assumed that characterizes the interior self-gravitating fluid distribution. We have considered that the sphere is originally filled with an isotropic matter and then added a Lagrangian density analogous to an extra fluid source, generating anisotropy in the original perfect fluid. We have added another source such that both the fluid sources are gravitationally coupled to each other. We have then observed that the field equations now possess the effects of both matter distributions that ultimately increase the degrees of freedom, and thus, a systematic approach must be needed to solve them. We have applied a transformation on the radial component (provided by MGD strategy) in the field equations that split them into two distinct systems. Each of these sets characterizes their parent (perfect and additional) sources, and we have solved them independently.

Firstly, we have dealt with the two independent field equations associated with the perfect fluid configuration. We have observed that the isotropic system contain four unknowns, therefore, the Finch-Skea metric has been adopted as a perfect fluid solution to the corresponding equations of motion. The temporal/radial components of this metric are given by

$$e^{a_1(r)} = \frac{1}{4}(2C_1 + C_2\sqrt{C_3r^2})^2, \quad e^{a_2(r)} = C_3r^2 + 1,$$

comprising a triplet of unknowns (C_1, C_2, C_3) . We have then considered the Schwarzschild exterior solution to match with the interior spherical metric and calculated these constants at the interface $\Sigma : r = R$. On the other hand, the field equations (22)-(24) representing an extra source also involve four unknowns including a matter triplet and the deformation function. We have tackled them by implementing three different constraints on E-sector separately, leading to distinct solutions. After solving both sets of equations, we have determined effective matter variables and anisotropy through the relations (25) and (26).

In order to ensure the physical relevancy of the developed models, we have investigated several factors through the graphical interpretation. We have chosen different values of the parameters such as $\xi = 0.25, 0.5, 0.75, 1$ and $\zeta = 0.1, 0.2, 0.3$ to check that how the interior fluid distribution is affected by the modified corrections and MGD scheme. The matter triplet corresponding to all three models have been observed acceptable for every parametric choice. We have found in each case that the lower values of ξ and ζ lead to more dense structure. Furthermore, we have plotted dominant energy conditions that ensure the presence of usual matter in the interior of each proposed model. With reference to the stability analysis, we have implemented the causality conditions and cracking criterion on the resulting solutions. It is found that our models I and II are stable for all chosen values of the model and decoupling parameters. However, model III is stable only for $\zeta = 0.1$ and 0.2 because the tangential sound speed criterion has not been fulfilled for $\zeta = 0.3$. It must be acknowledged here that our results regarding models I and II are better than that produced in the context of GR [29]. Moreover, our model II is compatible with the anisotropic Tolman VII [63] as well as Buchdahl's solutions [64]. It must be mentioned here that putting $\xi = 0$ reduces all these results to GR.

Finally, we have also compared our developed results with the observational data. For this, we have presented numerical data for each solution in

Tables 1-9. The energy density has been found to be of order 10^{14} or 10^{15} , which is consistent with the requirement for the existence of compact stars. Since we have considered a compact candidate LMC X-4, the observed and calculated masses of this star are in agreement with each other. The calculated values are given as

- $M = 1.08\mathcal{M}_{\odot}$, $1.06\mathcal{M}_{\odot}$ and $1.09\mathcal{M}_{\odot}$ for $\xi = 0.25$ and $\zeta = 0.1$ corresponding to model I, II and III, respectively.
- $M = 0.96\mathcal{M}_{\odot}$, $1.03\mathcal{M}_{\odot}$ and $0.95\mathcal{M}_{\odot}$ for $\xi = 0.25$ and $\zeta = 0.2$ corresponding to model I, II and III, respectively.
- $M = 0.83\mathcal{M}_{\odot}$, $1.04\mathcal{M}_{\odot}$ and $0.87\mathcal{M}_{\odot}$ for $\xi = 0.25$ and $\zeta = 0.3$ corresponding to model I, II and III, respectively.

It has been observed from the above discussion that the lower values of both model and decoupling parameters produce a best fit to the existing data.

Data Availability Statement: This manuscript has no associated data.

References

- [1] Capozziello, S. et al.: *Class. Quantum Grav.* **25**(2008) 085004.
- [2] Nojiri, S. et al.: *Phys. Lett. B* **681**(2009)74.
- [3] de Felice, A. and Tsujikawa, S.: *Living Rev. Relativ.* **13**(2010)3.
- [4] Nojiri, S. and Odintsov, S.D.: *Phys. Rep.* **505**(2011)59.
- [5] Astashenok, A.V., Capozziello, S. and Odintsov, S.D.: *J. Cosmol. Astropart. Phys.* **01**(2015)001.
- [6] Astashenok, A.V., Capozziello, S. and Odintsov, S.D.: *Phys. Lett. B* **742**(2015)160.
- [7] Bertolami, O. et al.: *Phys. Rev. D* **75**(2007)104016.
- [8] Harko, T. et al.: *Phys. Rev. D* **84**(2011)024020.
- [9] Deng, X.M. and Xie, Y.: *Int. J. Theor. Phys.* **54**(2015)1739.

- [10] Houndjo, M.J.S.: *Int. J. Mod. Phys. D* **21**(2012)1250003.
- [11] Nashed, G.G.L.: *Astrophys. J.* **950**(2023)129.
- [12] Singh, K.N. et al.: *Phys. Dark Universe* **30**(2020)100620.
- [13] Maurya, S.K.: *Phys. Dark Universe* **30**(2020)100640.
- [14] Rej, P., Bhar, Piyali. and Govender, M.: *Eur. Phys. J. C* **81**(2021)316.
- [15] Kaur, S., Maurya, S.K., Shukla, S. and Nag, R.: *Chin. J. Phys.* **77**(2022)2854.
- [16] Sharif, M. and Naseer, T.: *Eur. Phys. J. Plus* **137**(2022)1304.
- [17] Schwarz, D.J. and Weinhorst, B.: *Astron. Astrophys.* **474**(2007)717.
- [18] Antoniou, I. and Perivolaropoulos, L.: *J. Cosmol. Astropart. Phys.* **12**(2010)012.
- [19] Colin, J., Mohayaee, R., Sarkar, S. and Shafieloo, A.: *Mon. Not. R. Soc.* **414**(2011)264.
- [20] Javanmardi, B., Porciani, C., Kroupa, P. and Pflamm-Altenburg, J.: *Astrophys. J.* **810**(2015)47.
- [21] Tiwari, P. and Nusser, A.: *J. Cosmol. Astropart. Phys.* **3**(2016)062.
- [22] Řípa, J. and Shafieloo, A.: *Astrophys. J.* **851**(2017)15.
- [23] Migkas, K. and Reiprich, T.H.: *Astron. Astrophys.* **611**(2018)A50.
- [24] Migkas, K. et al.: *Astron. Astrophys.* **636**(2020)A15.
- [25] Ovalle, J.: *Mod. Phys. Lett. A* **23**(2008)3247.
- [26] Ovalle, J. and Linares, F.: *Phys. Rev. D* **88**(2013)104026.
- [27] Casadio, R., Ovalle, J. and Da Rocha, R.: *Class. Quantum Grav.* **32**(2015)215020.
- [28] Ovalle, J. et al.: *Eur. Phys. J. C* **78**(2018)960.
- [29] Sharif, M. and Sadiq, S.: *Eur. Phys. J. C* **78**(2018)410.

- [30] Gabbanelli, L., Rincón, Á. and Rubio, C.: Eur. Phys. J. C **78**(2018)370.
- [31] Estrada, M. and Tello-Ortiz, F.: Eur. Phys. J. Plus **133**(2018)453.
- [32] Hensh, S. and Stuchlík, Z.: Eur. Phys. J. C **79**(2019)834.
- [33] Sharif, M. and Naseer, T.: Chin. J. Phys. **73**(2021)179.
- [34] Sharif, M. and Naseer, T.: Int. J. Mod. Phys. D **31**(2022)2240017.
- [35] Naseer, T. and Sharif, M.: Universe **8**(2022)62.
- [36] Finch, M.R. and Skea, J.E.F.: Class. Quantum Grav. **6**(1989)467.
- [37] Banerjee, A. et al: Gen. Relativ. Gravit. **45**(2013)717.
- [38] Hansraj, S. and Maharaj, S.D.: Int. J. Mod. Phys. D **15**(2006)1311.
- [39] Bhar, P. et al: Int. J. Mod. Phys. D **26**(2017)1750078.
- [40] Shamir, M.F., Mustafa, G. and Ahmad, M.: Nucl. Phys. B **967**(2021)115418.
- [41] Dey, S., Chanda, A. and Paul, B.C.: Eur. Phys. J. Plus **136**(2021)228.
- [42] Ashmita, Sarkar, P. and Das, P.K.: Int. J. Mod. Phys. D **31**(2022)2250120.
- [43] Kaur, S., Maurya, S.K., Shukla, S. and Nag, R.: Chin. J. Phys. **77**(2022)2854.
- [44] Sharif, M. and Naseer, T.: Class. Quantum Grav. **40**(2023)035009.
- [45] Naseer, T. and Sharif, M.: Fortschr. Phys. **71**(2023)2300004.
- [46] Buchdahl, H.A.: Phys. Rev. **116**(1959)1027.
- [47] Clifton, T. et al.: Phys. Rev. D **87**(2013)063517.
- [48] Goswami, R. et al.: Phys. Rev. D **90**(2014)084011.
- [49] Delgaty, M.S.R. and Lake, K.: Comput. Phys. Commun. **115**(1998)395.
- [50] Ivanov, B.V.: Eur. Phys. J. C **77**(2017)738.

- [51] Ivanov, B.V.: Phys. Rev. D **65**(2002)104011.
- [52] Abreu, H., Hernandez, H. and Nunez, L.A.: Class. Quantum Grav. **24**(2007)4631.
- [53] Herrera, L.: Phys. Lett. A **165**(1992)206.
- [54] Heras, C.L. and León, P.: Fortschr. Phys. **66**(2018)1800036.
- [55] Gangopadhyay, T., Ray, S., Xiang-Dong, L., Jishnu, D. and Mira, D.: Mon. Not. R. Astron. Soc. **431**(2013)3216.
- [56] Carvalho, G.A. et al.: Eur. Phys. J. C **77**(2017)81.
- [57] Pretel, J.M.Z. et al.: J. Cosmol. Astropart. Phys. **04**(2021)064.
- [58] Bora, J. and Goswami, U.D.: Phys. Dark Universe **38**(2022)101132.
- [59] Pretel, J.M.Z.: Mod. Phys. Lett. A **37**(2022)2250188.
- [60] da Silva, F.M. et al.: Eur. Phys. J. C **83**(2023)295.
- [61] Graterol, R.P.: Eur. Phys. J. Plus **133**(2018)244.
- [62] Contreras, E. and Bargueño, P.: Class. Quantum Grav. **36**(2019)215009.
- [63] Azmat, H. and Zubair, M.: Eur. Phys. J. Plus **136**(2021)112.
- [64] Naseer, T. and Sharif, M.: Phys. Scr. **99**(2024)035001.